Pergamon

Int. J. Heat Mass Transfer. Vol. 38, No. 1, pp. 23–30, 1995

0017-9310/95 $9.50+0.00

0017-9310(94)00147-2

The anisotropic overall thermal conductivity induced by preferentially oriented pores

DA YU TZOU

Department of Mechanical Engineering, The University of New Mexico, Albuquerque, NM 87131, U.S.A.

(*Received* 28 *February* 1994 *and in final form* 16 *May* 1994)

Abstract—The differential formulation employing a self-consistent concept is extended to study the directional response of overall thermal conductivity in a porous medium containing anisometric pores. The anisometric pores distribute in a special direction relative to the incoming heat flux vector, rendering an anisotropic overall thermal conductivity tensor when discharging the heat flow in the porous medium. Cylindrical cavities with insulated surfaces are exemplified in the numerical example, demonstrating the directional response. Effects of the preferential orientation and the aspect ratio of the cylindrical cavities on the anisotropy of the overall thermal conductivity tensor are studied.

INTRODUCTION

Cavities or pores in a solid may be present in two ways: those resulting from natural consequences such as microcracks in rocks or microvoids in concrete, and those from artificial means such as load-induced damage in ceramic composites. In the former category, including powder metallurgical materials, internal cavities are produced in a natural fashion, implying that the cavities are randomly oriented in *all* directions in the porous medium. This is the physical basis for the traditional lumped formulation emphasizing the geometrical alignment of the pore and the matrix material in terms of serial or parallel combinations. In the latter category, on the other hand, orientations of the internal cavities depend on the way in which load is transmitted through the medium, implying that the spatial distributions and orientations of the internal cavities are restricted in a certain physical domain. Typical examples include microcracks induced by externally applied compression and delaminations along the interface between matrix material and second-phase strengthening fibers. A tensile hoop stress, as is well known, is produced in the direction perpendicular to that of compression. Such a tensile stress may break the local intergranular bounds, producing microcracks in the direction parallel to the compression in an overall (or averaged) sense. The complicated microstructure among grains is a decisive factor determining the amount of deviation (of the microcrack orientations) from the direction of the load. Delaminations along the interface between the matrix material and the strengthening fibers in the second example follow the spatial orientations of the fibers. When thermal energy is redistributed by these internal structures, clearly these cavities oriented in a special way would induce a directional response measured by the overall thermal conductivity *tensor*.

The random orientation of internal pores in all directions is a popular assumption made in the lumped formulation for the estimate of the overall thermal conductivity [1–5]. Inherited from such a simplification, the resulting overall thermal conductivity is *isotropic*, which makes it possible to study other complicated mechanisms, such as the temperature-dependence of the effective thermal conductivity at elevated temperatures [6, 7]. The overall thermal conductivity in porous media containing randomly oriented pores, evidenced by the large volume of publication in the past two decades, has been well-understood. Many existing models seem to provide accurate predictions when compared to experimental data under the same assumption. One of the most important characteristics revealed by past research is that the overall thermal conductivity should be regarded as a *structural* property rather than an intrinsic thermal property of the material. For the case of randomly oriented pores in a matrix material, for example, the overall thermal conductivity strongly depends on the *internal* heat transfer across the pore surfaces [8]. The overall thermal conductivity, in other words, is a property reflecting the combined effect of thermal loading (including the internal heat transfer), geometry of pores and the intact thermal conductivity of the matrix material. In conjunction with the increasing desire of precision control for heat transfer in porous media, the analytical model should be able to reflect such a complicated interactions among the three factors.

The present work extends the differential formulation [8, 9] to study the directional response of

NOMENCLATURE

a	characteristic dimension of the internal cavity [mm]
b	characteristic dimension of the spheroidal cavity [mm]
f	volume fraction of internal cavities
G	Green's functions in the anisotropic medium
H	added tensor in the overall thermal resistance tensor [m K W^{-1}]
K	common magnitude in the thermal conductivity tensor [W m^{-1} K^{-1}]
k	thermal conductivity [W m^{-1} K^{-1}]
N	total number of cavities per unit volume
n	unit normal to the cavity surface
Q	associated heat flux vector in the boundary element method [W m^{-2}]
q	heat flux vector [W m^{-2}]
R	thermal resistance [m K^{-1} W^{-1}]
r	geodesic distance defined by equation (16) [$(m^3$ K $W^{-1})^{1/2}$]. Radial distance [mm]
S	surface area
T	temperature [K]
V	volume [m^3]
x	spatial coordinates of the field point [mm]
y	spatial coordinate of the observation point [mm].

Greek symbols

β	transformation matrix between the prime and the global coordinates
δ	Kronecker delta function
Θ, Φ	spherical coordinates in the prime coordinate system [°]
ϑ, φ	Euler angles between the prime and the global coordinate systems [°].

Subscripts and superscripts

C	quantities in the cavity
D	the disturbance component (by cavities)
i, j	components in the x_i direction, $i, j = 1, 2, 3$
M	quantities in the matrix
P	the primary component
q	the heat flux component
T	the temperature component
$\bar{X}$	the volumetric average
X'	quantities in the prime (self-consistent) coordinate system
X^*	dimensionless quantities normalized with respect to the corresponding intact values
X^{-1}	matrix inverse
$\|X\|$	determinant
0	orientation angle of internal pores.

the overall thermal conductivity in a porous medium. Subjecting to the impingement of an incoming heat flux vector, the source of *anisotropy* lies in the preferential orientations of internal cavities, which are assumed uniformly distributed in a matrix material. Because the orientations of these cavities are restricted in certain physical domains, re-distribution of heat flow by these cavities is expected to display a stronger dependence on directions. The *anisotropic* overall thermal conductivity *tensor* derived in this work is to quantify such a directional response. The internal heat transfer across the pore surfaces is an important factor affecting the overall thermal conductivity in porous media. For a better focus on the geometrical effect of preferentially oriented pores on the overall thermal conductivity, however, all the cavities shall be assumed *insulated* at this stage of exploration.

THE DIFFERENTIAL FORMULATION

Figure 1(a) describes the cylindrical cavities uniformly distributed in a matrix material. With regard to the orientations of these cavities, however, they are confined to a conical domain of $2\varphi_0$. The advantage of the self-consistent concept [8–13], as illustrated in Fig. 1(b), lies in the assumed *equivalence* between the self-consistent system, including a *single* but *representative* cavity, and the real system, containing hundreds and thousands of real cavities. The thermal conductivity (resistance) tensors of the cavity and the matrix phases in the real system are, respectively, k_{ij}^{C} (R_{ij}^{C}) and k_{ij}^{M} (R_{ij}^{M}), while that in the self-consistent system where the representative cavity is located is $\bar{k}_{ij}$ ($\bar{R}_{ij}$). $\bar{k}_{ij}$ is the overall (or effective) thermal conductivity tensor, the primary quantity to be sought for heat conduction through porous media. The differential formulation [8, 9] absorbs the effect of internal cavities in an *added* tensor, H_{ij}, in the overall thermal resistance tensor:

$$\bar{R}_{ij} = R_{ij} + H_{ij}(\bar{R}_{ij}) \quad \text{with}$$
$$\bar{k}_{ij} = \bar{R}_{ij}^{-1} \quad \text{and} \quad k_{ij} = R_{ij}^{-1}. \tag{1}$$

Should the H_{ij} tensor be determined, equation (1) can be used to solve the individual components of $\bar{R}_{ij}$. The overall thermal conductivity tensor, $\bar{k}_{ij}$, is then the simple matrix inversion of $\bar{R}_{ij}$. In order to determine the H_{ij} tensor, it is necessary to determine the H'_{ij} tensor in the prime coordinate system. The prime coordinates x'_i for $i = 1, 2, 3$, as shown in Fig. 1(b),

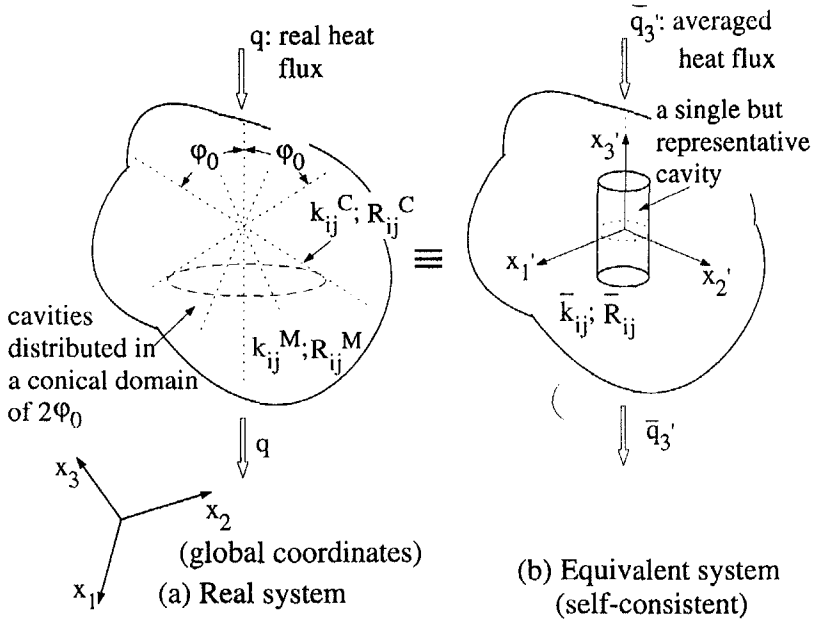

Fig. 1. Equivalence between (a) the real system containing preferentially oriented cavities in a conical domain of $2\varphi_0$, and (b) the self-consistent system containing a single but representative cavity.

are introduced to describe heat transport in the self-consistent system. The x_3'-axis is aligned with the incoming heat flux averaged over the entire volume of the porous medium:

$$\bar{q}_3' = \frac{1}{V}\int_V q_3'(x_j)\,\mathrm{d}V. \tag{2}$$

Relative to the *global* coordinate system x_i, as shown in Fig. 2 with more details, the prime coordinates are defined by two Euler angles ϑ and φ. The H_{ij}' tensor, as derived in refs. [8, 9], is the temperature averaged over the entire surface of the representative cavity in the self-consistent system:

$$H_{ij}' = \int_{S^C} \frac{T(x_k')}{\bar{q}_j'} n_i'(x_k')\,\mathrm{d}S^C \quad \text{for} \quad i, j, k = 1, 2, 3 \tag{3}$$

where $n_i'(x_k')$ is the unit normal along the cavity surface, which varies from one location to another for anisometric pores. The H_{ij} tensor is then the spatial *average* of the H_{ij}' tensor over the possible domains of ϑ and φ, describing the cavity orientations,

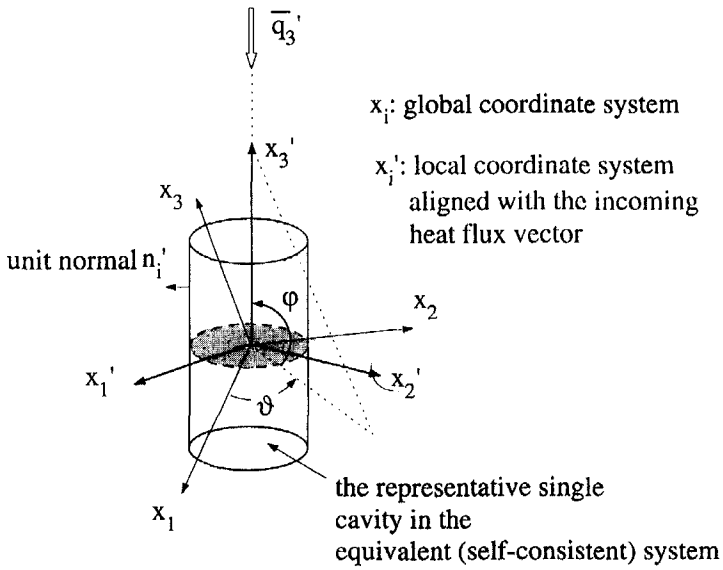

Fig. 2. The prime coordinate system describing the overall response in the self-consistent system and its relative orientations to the global coordinate system.

$$H_{ij} = \frac{N}{(\vartheta_2 - \vartheta_1)} \int_{\vartheta_1}^{\vartheta_2} \int_{\varphi_1}^{\varphi_2} \beta_{im}\beta_{jn} H'_{mn}(\bar{R}_{ij}) \cos\varphi \, d\varphi \, d\vartheta \tag{4}$$

where (Fig. 2) β_{ij} is the matrix of direction cosines between x'_i and x_j:

$$\beta_{ij} = \begin{bmatrix} -\sin\vartheta & -\sin\varphi\cos\vartheta & \cos\varphi\cos\vartheta \\ \cos\vartheta & -\sin\varphi\sin\vartheta & \cos\varphi\sin\vartheta \\ 0 & \cos\varphi & \sin\varphi \end{bmatrix}. \tag{5}$$

For cylindrical cavities restricted in the conical domain of $\varphi \in [0, \varphi_0]$ [Fig. 1(a)], while uniformly oriented in the ϑ-direction, $\vartheta \in [0, 2\pi]$, equation (4) reduces to

$$H_{ij} = \frac{N}{2\pi} \int_0^{2\pi} \int_{\varphi_1}^{\varphi_2} \beta_{im}\beta_{jn} H'_{mn}(\bar{R}_{ij}) \cos\varphi \, d\varphi \, d\vartheta. \tag{6}$$

With the assistance of equation (6), therefore, equation (1) can be used to solve the individual components of $\bar{R}_{ij}$. For porous media containing spherical pores and penny-shaped cracks [8, 9], the differential model has been applied to study the effects of cavity geometry and the internal heat transfer across the cavity surfaces. Excellent agreement with the experimental data results for porosity, going all the way up to 46%, the largest value of porosity in the experiment of ref. [7].

BOUNDARY ELEMENT FORMULATION

Temperature distribution on the surface of the representative cavity, as reflected by equation (3), is a decisive quantity determining the overall thermal conductivity (resistance) tensor in the differential formulation. With regard to the present problem, involving a cylindrical cavity in an anisotropic material, a closed-form solution for temperature does not exist and a numerical method is needed. The boundary-element technique is more suitable for the present problem because (i) it does not require a field mesh (thus superior to the finite element method) for obtaining the surface temperature, and (ii) the Green's function needed for the *exterior* formulation is readily available.

The temperature and the heat flux fields in the prime coordinates established on the cylindrical cavity, Fig. 2, can be decomposed into the primary $^{(P)}$ and the disturbance $^{(D)}$ components:

$$T = T^{(P)} + T^{(D)} \quad \text{and} \quad Q_i = Q_i^{(P)} + Q_i^{(D)} \quad \text{for} \quad i = 1, 2, 3. \tag{7}$$

The primary components, $T^{(P)}$ and $Q_i^{(P)}$, absorb the effect of the incoming heat flux $\bar{q}_3$,

$$T^{(P)} = [\bar{R}_{31}x'_1 + \bar{R}_{32}x'_2 + \bar{R}_{33}x'_3]\bar{q}'_3, \quad \text{consequently}$$
$$Q_1^{(P)} = Q_2^{(P)} = 0; \quad Q_3^{(P)} = -\bar{q}'_3 \tag{8}$$

while the disturbance components, $T^{(D)}$ and $Q_i^{(D)}$, satisfy

$$\bar{k}_{11}\frac{\partial^2 T^{(D)}}{\partial x_1'^2} + \bar{k}_{22}\frac{\partial^2 T^{(D)}}{\partial x_2'^2} + \bar{k}_{33}\frac{\partial^2 T^{(D)}}{\partial x_3'^2} + (\bar{k}_{12} + \bar{k}_{21})\frac{\partial^2 T^{(D)}}{\partial x'_1 \partial x'_2} + (\bar{k}_{23} + \bar{k}_{32})\frac{\partial^2 T^{(D)}}{\partial x'_2 \partial x'_3} + (\bar{k}_{13} + \bar{k}_{31})\frac{\partial^2 T^{(D)}}{\partial x'_1 \partial x'_3} = 0 \tag{9}$$

and

$$Q_i^{(D)} = -\bar{k}_{ij}\frac{\partial T^{(D)}}{\partial x'_j} \quad \text{for} \quad i, j = 1, 2, 3. \tag{10}$$

At a large distance away from the cavity, the regular condition for the temperature disturbance is imposed:

$$T^{(D)} = 0 \quad \text{as} \quad \sqrt{(x_1'^2 + x_2'^2 + x_3'^2)} \to \infty. \tag{11}$$

At the cavity surface, on the other hand, an insulated condition is assumed:† $Q_i n'_i = 0$ for $i = 1, 2, 3$. For heat flow through an anisotropic medium [14], $-Q_i = \bar{k}_{ij}(\partial T/\partial x_j)$. In an unabridged form, it reads

$$\left(\bar{k}_{11}\frac{\partial T}{\partial x'_1} + \bar{k}_{12}\frac{\partial T}{\partial x'_2} + \bar{k}_{13}\frac{\partial T}{\partial x'_3}\right)n'_1 + \left(\bar{k}_{21}\frac{\partial T}{\partial x'_1} + \bar{k}_{22}\frac{\partial T}{\partial x'_2} + \bar{k}_{23}\frac{\partial T}{\partial x'_3}\right)n'_2 + \left(\bar{k}_{33}\frac{\partial T}{\partial x'_1} + \bar{k}_{32}\frac{\partial T}{\partial x'_2} + \bar{k}_{33}\frac{\partial T}{\partial x'_3}\right)n'_3 = 0. \tag{12}$$

With the assistance of equation (8), equation (12) results:

$$Q_1^{(D)} = Q_2^{(D)} = 0 \quad \text{and} \quad Q_3^{(D)} = \bar{q}'_3 \quad \text{for} \quad x'_i \in S^C. \tag{13}$$

The disturbance component of temperature satisfying equation (9) and the boundary conditions (11) and

† The quantity $Q_i n'_i$ is the projection of the associated heat flux vector onto the normal direction of the surface element with a unit normal n'_i. Should the conduction–convection model of internal heat transfer across the pore surface be considered, equation (12) becomes

$$\left(\bar{k}_{11}\frac{\partial T}{\partial x'_1} + \bar{k}_{12}\frac{\partial T}{\partial x'_2} + \bar{k}_{13}\frac{\partial T}{\partial x'_3}\right)n'_1 + \left(\bar{k}_{21}\frac{\partial T}{\partial x'_1} + \bar{k}_{22}\frac{\partial T}{\partial x'_2} + \bar{k}_{23}\frac{\partial T}{\partial x'_3}\right)n'_2 + \left(\bar{k}_{33}\frac{\partial T}{\partial x'_1} + \bar{k}_{32}\frac{\partial T}{\partial x'_2} + \bar{k}_{33}\frac{\partial T}{\partial x'_3}\right)n'_3 = hT$$

with h being the averaged value of the heat transfer coefficient in the prime coordinate system. Physically, assuming insulated cavities will *underestimate* the overall thermal conductivity, especially in the high-porosity domain [8]. The insulated cavities assumed in this work illustrate the fundamental procedure in the *simplest* case. The internal heat transfer across the pore surface can be accommodated by replacing the right side of equation (12) by hT in the boundary-element calculations.

(13) can be arranged into an integral equation. The weighting functions are given by the free space Green's functions, $G^{T}(x_i'y_i')$ for temperature and $G_k^q(x_i'y_i')$ for the corresponding heat flux vector [15]:

$$\tfrac{1}{2}T^{(D)}(x_i') + \int_{S^C} G_k^q(x_i'|y_i')\, T^{(D)}(y_i')n_k'(y_i')\,dS^C = \int_{S^C} G^T(x_i'|y_i')\, Q_k(y_i')n_k'(y_i')\,dS^C \quad (14)$$

where x_i' and y_i' for $i = 1, 2, 3$ are, respectively, the field point inside the equivalent medium and the observation point on the cavity surface. The unit normal n_i' and the differential surface S^C, consequently, are functions of y_i'. The three-dimensional Green's function for $G^T(x_i'|y_i')$ in equation (18) has been derived [16]:

$$G^T(x_i'|y_i') = \frac{\sqrt{|\bar{R}_{ij}|}}{4\pi r} \quad (15)$$

with $|\bar{R}_{ij}|$ denoting the determinant of the $\bar{R}_{ij}$ tensor and r, the geodesic distance, defined by

$$r = \sqrt{[\bar{R}_{ij}(x_i'-y_i')(x_j'-y_j')]} \quad \text{for} \quad i,j = 1,2,3. \quad (16)$$

The Green's function for $G_k^q(x_i'|y_i')$ can thus be derived accordingly:

$$G_k^q = -\bar{k}_{ij}\frac{\partial G^T}{\partial x_k'}, \quad \text{implying}$$

$$G_k^q n_k' = \frac{(x_i'-y_i')n_i'\sqrt{|\bar{R}_{ij}|}}{4\pi r^3}. \quad (17)$$

The unit normals n_i' of the cavity surface are involved in both equation (3) for the H_{ij}' tensor and the integral equation (14), governing the disturbance temperature $T^{(D)}$. Numerically, it can be expressed in terms of the nodal coordinates of the boundary elements [15].

The integral equation (14) is discretized by the standard boundary-element approximations. As shown in Fig. 3 for a typical boundary element mesh, both quadrilateral and triangular superparametric elements with constant functional approximation are used for this purpose. The discretization thus renders a system of linear algebraic equations to be solved for $T^{(D)}$ on the cavity surface:

$$\tfrac{1}{2}T_m^{(D)} + T_l^{(D)}M_{ml} = Q_i^l N_i^{ml} \quad (18)$$

where the superscripts and subscripts m denote the nodal values at the mth boundary element node, Q_i^m is the associated heat flux vector, and M_{ml} and N_i^{ml} result from the integrations of the kernel functions and the shape functions over each element. Since the $Q_i^{(D)}$ functions are specified on the cavity surface, refer to equation (13), equation (18) can be solved for the disturbance temperature $T_m^{(D)}$ at each boundary element node.

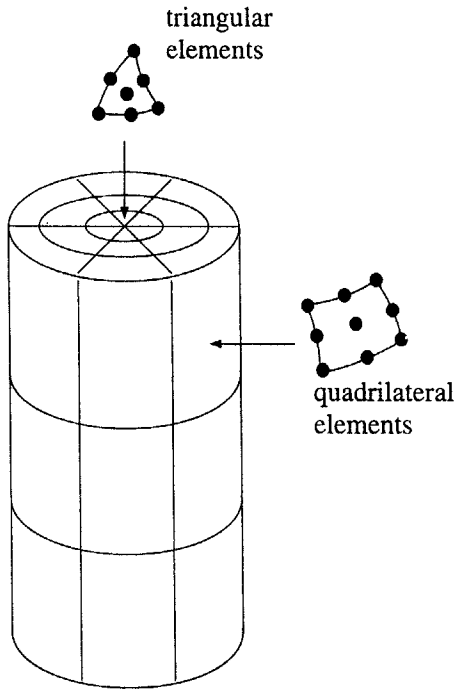

Fig. 3. Typical boundary element mesh of the representative cylindrical cavity and the triangular and the quadrilateral elements used in discretization.

THE ITERATION TECHNIQUE

Except for the three-dimensional Green's functions in an anisotropic material [equations (15) and (17)], the boundary element technique used in this analysis is quite standard. In determining the surface temperature of the cavity, however, the overall moduli, $\bar{R}_{ij}$ or $\bar{k}_{ij}$, in equations (8) and (14)–(17) are the primary *unknowns* to be determined. At the stage of determining the surface temperature, in other words, they are still unknown. An iterative scheme is thus developed to overcome this difficulty. The *overall* thermal resistance (conductivity) tensor in the equivalent (self-consistent) system is first assumed to be *identical* to the *intact* thermal resistance (conductivity) tensor, i.e.

$$\bar{k}_{ij}^{(0)} = k_{ij} \quad \text{and} \quad \bar{R}_{ij}^{(0)} = R_{ij}. \quad (19)$$

Based on such zeroth order approximations, the surface temperature is calculated by the boundary element method. Integrating numerically for the $H_{ij}'^{(0)}$ tensor according to equation (3), and the $H_{ij}^{(0)}$ tensor according to equation (6), results in

$$H_{ij}^{(0)} \equiv H_{ij}^{(0)}(\bar{R}_{ij}^{(0)}). \quad (20)$$

Substituting equation (20) into equation (1), the *first*-order approximation for the overall thermal resistance (conductivity) tensor results:

$$\bar{R}_{ij}^{(1)} = R_{ij} + H_{ij}(\bar{R}_{ij}^{(0)}), \quad \bar{k}_{ij}^{(1)} = [\bar{R}_{ij}^{(1)}]^{-1}. \quad (21)$$

The newly obtained overall thermal resistance (conductivity) tensor is then used to determine the surface

temperature and calculate the second-order approximation for $\bar{R}_{ij}^{(2)}$ and $\bar{k}_{ij}^{(2)}$ in the same manner. The iteration continues until the change of the components in the overall conductivity tensor is less than a prescribed threshold. Such an iterative scheme, as shown later, results in a rapid convergence for the present problem.

NUMERICAL EXAMPLES OF SELECTED CASES

The directional response induced by the cylindrical cavities oriented in a conical angle of $\varphi_0 = 30°$ is first studied. The radius, a, and length, l, of the representative cavity are, respectively, 1 and 2 mm. The thermal conductivity tensor for the matrix material is assumed to be

$$k_{ij} = \begin{bmatrix} 2 & 0.1 & 0.3 \\ 0.1 & 2 & 0.4 \\ 0.3 & 0.4 & 1 \end{bmatrix} K \tag{22}$$

which is normalized with respect to the k_{33} component. The amount of anisotropy induced by the preferentially oriented pores depends on the intact thermal conductivity tensor. The particular components in equation (22) are selected for obtaining a more exaggerated directional response in the overall thermal conductivity tensor. Simpler cases such as an isotropic or orthotropic conductivity tensor can be equally well selected as the basis of the analysis, but the difference among the components in the resulting overall thermal conductivity tensor may not be as pronounced. The value of K can be arbitrarily chosen because the overall thermal conductivity tensor, $\bar{k}_{ij}$, shall be obtained relative to the individual components of k_{ij}:

$$k_{ij}^* = \frac{\bar{k}_{ij}}{k_{ij}} \quad \text{for} \quad i,j = 1,2,3. \tag{23}$$

For $f = Na^3 = 0.5$, Fig. 4 shows the rapid convergence of the k_{ij}^* components when the number of elements discretizing the cavity surface increases. A desirable *uniform* convergence results for all the components of k_{ij}^*. The number of elements is thus fixed at 45, which

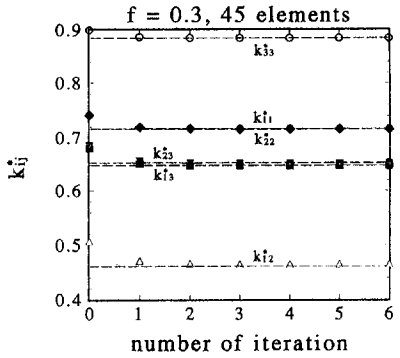

Fig. 5. Convergence of the k_{ij}^* components with increase of the number of iterations. $f = 0.3$ and 45 elements, $\varphi_0 = 60°$, $a = 1$ mm and $l = 2$ mm.

is sufficient for all the analyses in this work. Figure 5 shows convergence of the k_{ij}^* tensor with the number of iterations: refer to equations (19)–(21) for the successive approximations of the overall thermal resistance tensor. For all the analyses performed in this work, the iteration continues until the difference between two successive approximations, say $\bar{R}_{ij}^{(i)} - \bar{R}_{ij}^{(i-1)}$, is less than 10^{-5} compared to the previous value of $\bar{R}_{ij}^{(i-1)}$. With numerical convergence thus examined, Fig. 6 displays the variations of the k_{ij}^* components with the volume fraction ($f = Na^3$) of the cylindrical cavities. A strong directional response results, as reflected by the different values of the k_{ij}^* components at various values of f. The *anisotropic* overall thermal conductivity tensor remains symmetric. The preferential orientations of the internal cavities, most importantly, introduce a *nonlinear* effect in the distributions vs the volume fraction. The k_{33}^* component experiences the least amount of degradation [because the area reduction associated with the variation of orientations for $2\varphi_0 = 60°$ is least in the direction of x_3, refer to Fig. 1(a)], while the component k_{12}^* suffers a more serious degree of degradation. The *linear* isotropic response [17] is enclosed for comparison. Along with the other components of k_{ij}^*, the isotropic distribution is bounded by the curves

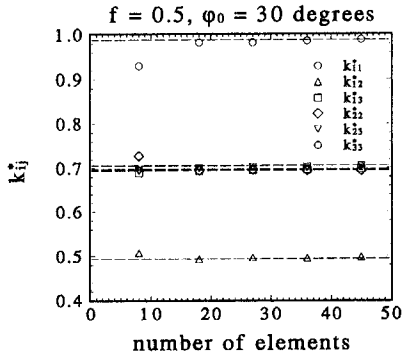

Fig. 4. Convergence of the k_{ij}^* components with increase of the boundary elements. $f = 0.5$, $\varphi_0 = 30°$, $a = 1$ mm and $l = 2$ mm.

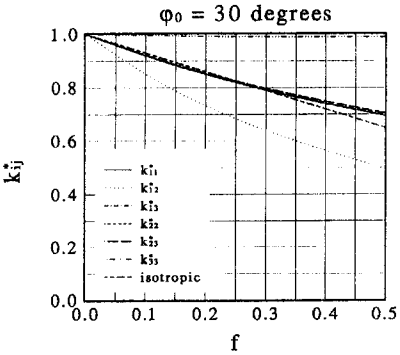

Fig. 6. Nonlinear response of the anisotropic components of k_{ij}^* with the volume fraction parameter. $\varphi_0 = 30°$, $a = 1$ mm and $l = 2$ mm. Isotropic case corresponds to $\varphi_0 = 90°$.

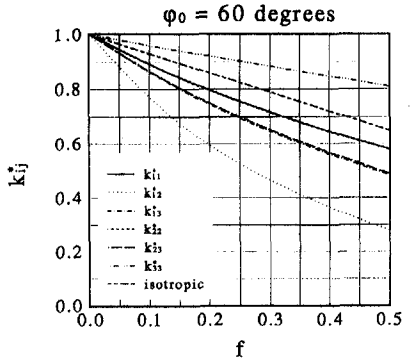

Fig. 7. Anisotropic components of k_{ij}^* varying as a function of the volume fraction parameter. $\varphi_0 = 30°$, $a = 1$ mm and $l = 2$ mm.

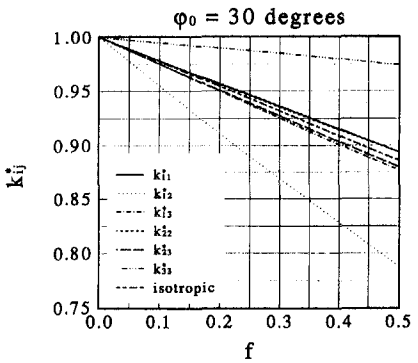

Fig. 8. Anisotropic components of k_{ij}^* varying as a function of the volume fraction parameter. Penny-shaped cavities with $\varphi_0 = 30°$, $a = 1$ mm and $l = 0.1$ mm.

of k_{33}^* and k_{12}^*. For the case of $\varphi_0 = 60°$, distributions of the k_{ij}^* components are shown in Fig. 7. Degradation becomes more pronounced for all components, due to larger domains of cavity orientations. Deviations among the k_{ij}^* components, especially for k_{11}^*, k_{13}^* and k_{23}^*, dramatically increase. The k_{11}^* and k_{22}^* components, however, remain close because the cavities are *uniformly* oriented in the ϑ-direction [refer to Figs. 1(a) and 2].

For a rather flat geometry with $a = 1$ mm and $l = 0.1$ mm, the case close to penny-shaped mesocracks [8, 9], Fig. 8 shows the distribution of k_{ij}^* for $\varphi_0 = 30°$. A smaller amount of degradation results compared with that in Fig. 6 for all components, because less area reduction is induced by the penny-shaped cavities. The results for $\varphi_0 = 60°$ are shown in Fig. 9. Again, larger degradation (for all components) and larger deviations (among k_{11}^*, k_{13}^* and k_{23}^*) result compared with those in Fig. 8. As shown by Figs. 6–9, the isotropic approximation is not appropriate, not even in the mean sense, should a directional response result from the preferential orientations in the cavity distribution. When the value of φ_0 approaches $\pi/2$ [Figs. 1(a) and (2) and equation (6)] with $\varphi_1 = -\pi/2$ and $\varphi_2 = \pi/2$, the overall conductivity tensor k_{ij}^* reduces to the isotropic value. For a typical value of $f = 0.5$ and $a = 1$ mm, this asymptotic behavior is shown in Fig. 10 (for $l = 2$ mm) and Fig. 11 ($l = 0.1$ mm). k_{33}^* is the only component which monotonically reduces to the isotropic value, while the other components "swing" to the isotropic value from below. Identity between the k_{11}^* and k_{22}^* components, to be reiterated, results from the uniform distribution of the cavities in the ϑ-direction. For cylindrical cavities, not only preferentially oriented in $\varphi \in [0, \pi/6]$, but also in $\vartheta \in [5\pi/6, 7\pi/6]$, as shown in Fig. 12 for the case of penny-shaped cavities ($a = 1$ mm and $l = 0.1$ mm), the distribution of k_{11}^* is no longer identical to that of k_{22}^*. Instead, k_{11}^* suffers much more pronounced degradation than k_{22}^*. Equation (4) with $\varphi_1 = 0$, $\varphi_2 = \pi/6$, $\vartheta_1 = 5\pi/6$ and $\vartheta_2 = 7\pi/6$ is used in this case. Compared to Fig. 8, where φ is in the same physical domain while ϑ is from 0 to 2π, an even stronger directional response results as reflected by the large deviations among all the components. The distributions of k_{ij}^* remain nonlinear, but become concave. The concave behavior implies degradation with a *faster* rate (with respect to f) in the domain, with larger values of porosity.

CONCLUSION

Heat transport through porous materials is a complicated subject depending on the internal structures of cavities in the matrix material. The overall (effective) thermal conductivity is a structural property reflecting the combined effect of thermal loading, geometrical configuration and spatial distributions of cavities and the relative thermal properties of the cavity and the matrix material. These three factors depict the way in which heat flow is re-distributed by the internal cavities. In most cases, however, the three factors are tangled together in a nonlinear fashion and they must be considered simultaneously. While other important characteristics of the overall thermal conductivity need to be further pursued, such as the irregular shapes of internal cavities [6] and the temperature-dependent behavior in a high temperature environment [6, 7], the present work has explored the

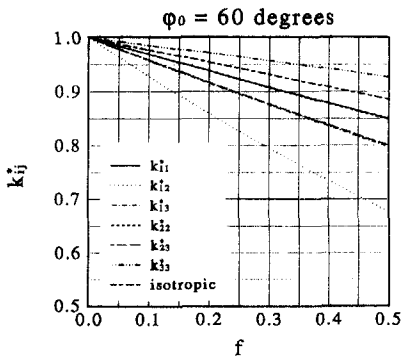

Fig. 9. Anisotropic components of k_{ij}^* varying as a function of the volume fraction parameter. Penny-shaped cavities with $\varphi_0 = 60°$, $a = 1$ mm and $l = 0.1$ mm.

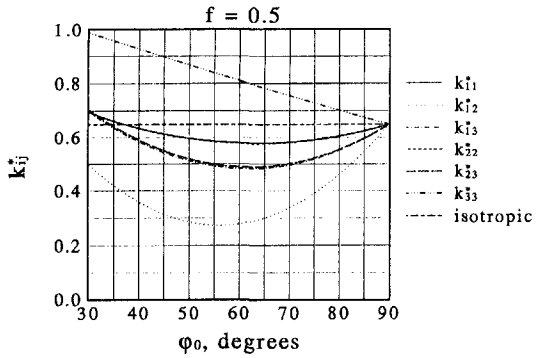

Fig. 10. Coalescence of the anisotropic overall thermal conductivity tensor to the isotropic value when the conical angle φ_0 approaches 90°. $f = 0.5$, $a = 1$ mm and $l = 2$ mm.

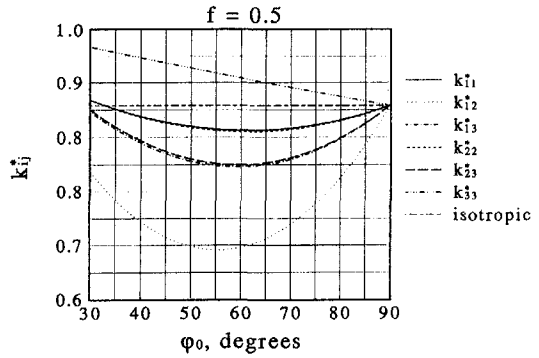

Fig. 11. Coalescence of the anisotropic overall thermal conductivity tensor to the isotropic value when the conical angle φ_0 approaches 90°. $f = 0.5$, $a = 1$ mm and $l = 0.1$ mm.

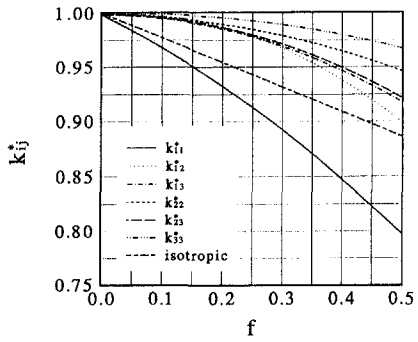

Fig. 12. Distributions of the k_{ij}^* components for penny-shaped cavities oriented in $\varphi \in [0, \pi/6]$ and $\vartheta \in [5\pi/6, 7\pi/6]$. $a = 1$ mm and $l = 0.1$ mm.

possible directional response induced by the internal cavities distributed with preferential orientations. Such a directional response, reflected by the anisotropic overall thermal conductivity tensor, significantly deviates from the isotropic response, as shown by Figs. 6–9. Figures 10 and 11 reveal the transition from an anisotropic to an isotropic response should the internal cavities become randomly and uniformly distributed in the porous medium. Due to complexity of the directional response, the boundary element method has been used to obtain the surface temperature of the representative cavity. The fast uniform convergence patterns, Figs. 4 and 5, support the feasibility of the method when used for such a purpose. The numerical computation is economical. In calculating the nine components of the overall thermal conductivity at $f = 0.5$, the most time-consuming case in this study, the execution time is about 90 s for 10 iterations. This data is based on the use of a 486-50 personal computer.

Acknowledgment—The author wishes to thank Dr Jing Li for his assistance in improving the numerical performance of the boundary element method when he was at the University of New Mexico.

REFERENCES

1. A. L. Loeb, Thermal conductivity: VIII. A theory of thermal conductivity of porous materials, *J. Am. Ceram. Soc.* **37**, 96–99 (1954).
2. S. C. Cheng and R. I. Vachon, The prediction of the thermal conductivity of two and three phase solid heterogeneous mixtures, *Int. J. Heat Mass Transfer* **12**, 249–264 (1969).
3. A. V. Luikov, A. G. Shashkov, L. L. Vasiliev and Y. E. Fraiman, Thermal conductivity of porous systems, *Int. J. Heat Mass Transfer* **11**, 117–140 (1968).
4. M. Kaviany, *Principles of Heat Transfer in Porous Media*. Springer, New York (1991).
5. M. Murabayashi, S. Namba, Y. Takahashi and T. Mukaibo, Effect of porosity on the thermal conductivity of ThO_2, *J. Nucl. Sci. Technol.* **6**, 128–131 (1969).
6. D. A. Zumbrunnen, R. Viskanta and F. P. Incropera, Heat transfer through porous solids with complex internal geometries, *Int. J. Heat Mass Transfer* **29**, 275–284 (1986).
7. J. S. Agapiou and M. F. DeVries, An experimental determination of the thermal conductivity of a 304L stainless steel powder metallurgy material, *ASME J. Heat Transfer* **111**, 281–286 (1989).
8. D. Y. Tzou, The effect of internal heat transfer in cavities on the overall thermal conductivity, *Int. J. Heat Mass Transfer* **34**, 1839–1846 (1991).
9. D. Y. Tzou and E. P. Chen, Overall degradation of conductivity solids with mesocracks, *Int. J. Heat Mass Transfer* **33**, 2173–2182 (1990).
10. B. Budiansky, Thermal and thermoelastic properties of isotropic composites, *J. Compos. Mater.* **4**, 286–295 (1970).
11. B. Budiansky, On the elastic moduli of some heterogeneous materials, *J. Mech. Phys. Solids* **13**, 223–227 (1965).
12. B. Budiansky and R. J. O'Connell, Elastic moduli of a cracked solid, *Int. J. Solids Structures* **12**, 81–97 (1976).
13. H. Horii and S. Nemat-Nasser, Overall moduli of solids with microcracks: load-induced anisotropy, *Int. J. Solids Structures* **31**, 155–171 (1983).
14. E. R. G. Eckert and R. M. Drake, Jr, *Analysis of Heat and Mass Transfer*, p. 14. McGraw-Hill, New York (1959).
15. C. A. Brebbia, J. C. F. Telles and L. C. Wrobel, *Boundary Element Techniques*. Springer, New York (1984).
16. Y. P. Chang, C. S. Kang and D. J. Chen, The use of fundamental Green's functions for the solution of problems of heat conduction in anisotropic media, *Int. J. Heat Mass Transfer* **16**, 1905–1918 (1973).
17. D. Y. Tzou and J. Li, Some scaling rules for the overall thermal conductivity in porous materials, *J. Compos. Mater.*, in press.